XVII International School on Nuclear Physics, Neutron Physics and Application, Sept. 24-30, 2007, Varna, Bulgaria

Role of fission in the r-process nucleosynthesis – needed input

Aleksandra Kelić and Karl-Heinz Schmidt
Gesellschaft für Schwerionenforschung, GSI, Planckstr. 1, D-64291 Darmstadt, Germany

Abstract. Fission determines the end-point of the astrophysical r-process and is expected to influence the nuclide abundances. Astrophysical network calculations require input on fission barriers of heavy r-process nuclei as well as mass- and element-distributions of the fission fragments. This manuscript reviews the status of present experimental and theoretical knowledge in this field. New methods are described and applied to make predictions on saddle-point masses and fission-fragment nuclide distributions for r-process nuclei.

Introduction

Different processes have contributed to the abundances of the nuclides we find in the Universe. While the Big Bang mostly left over hydrogen and helium, the synthesis of elements up to iron deliver the nuclear energy for stellar burning. The most important mechanisms for the production of heavier elements rely on neutron capture. Roughly, two processes can be distinguished, the “slow” s process and the “rapid” r process. Low neutron densities occur in suitable scenarios of stellar burning. After neutron capture, the nucleus falls back to a beta-stable nucleus by beta decay before another neutron is trapped. Thus, the s-process path leads along neutron-rich beta-stable nuclei. The s process necessarily stops at ^{209}Bi, because ^{211}Po, which is produced after beta decay of ^{210}Bi, decays back to ^{206}Pb by alpha decay. In supernovae or other explosive scenarios, very much higher neutron densities may occur, and consequently the time between two consecutive neutron-capture processes becomes much shorter. Thus, the r process proceeds via very neutron-rich nuclei far from the beta-stability valley. In the r process, fission can have an important influence on the abundances of long-lived actinides, which are relevant for determination of the age of the Galaxy and the Universe [1]. In scenarios where high neutron densities exist over long enough periods, fission has decisive influence on the termination of the r-process and production of super-heavy elements [2]. In similar scenarios, fission will influence the abundances of nuclei in the region A~90 and A~130 due to the fission cycling [3,4].
Studies on the role of fission in the r process began forty years ago [3]. Meanwhile, extensive investigations on beta-delayed, neutron- and neutrino-induced fission have been performed; see e.g. [4, 5, 6, 7, 8, 9]. One of the common conclusions from all this work is that the influence of fission on the r process is very sensitive to the fission-barrier heights of heavy r-process nuclei with A>190 and Z>84, since they determine the calculated fission probabilities of these nuclei. Moreover, information on mass- and element distributions of fragments formed in the fission of these heavy r-process nuclei is essential for calculations of r-process abundances.
In this contribution, we will concentrate on the status of experimental and theoretical knowledge on the fission process, which is needed as input for r-process calculations. We will discuss in details the heights of fission barriers and the fragment formation in fission. Firstly, using available experimental data on saddle-point and ground-state masses, we will present a dedicated study on the predictions of different models on the dependence of saddle-point masses on neutron excess [10]. Secondly, we will present a model for calculating mass- and element-distributions of fission fragments, which can correctly predict the transition from double-humped to single-humped distributions with decreasing mass of the fissionning system and increasing excitation energy in the light actinides. The results provide improved input for the role of fission in r-process network calculations.

Fission barriers

One of the most important ingredients for calculating fission probabilities is the height of the fission barrier. Unfortunately, experimental information on fission-barrier heights is only available for nuclei in a limited region of the nuclide chart, as shown in Figure 1.

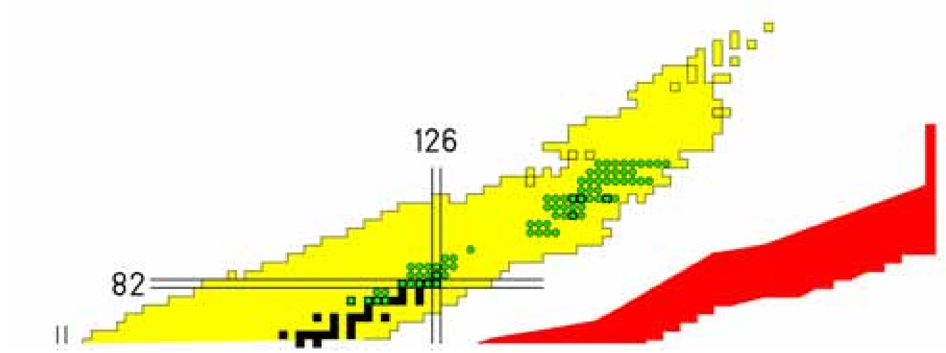

Figure 1. Available data (green dots) on fission barriers for $Z \geq 80$ taken from the RIPL-2 library [11] and shown on the nuclear chart. Black squares represent the stabile nuclei, and the red marked region a possible r-process path.

Therefore, for heavy r-process nuclei one has to rely on theoretically calculated barriers. Due to the limited number of available experimental barriers, in any theoretical model constraints on the parameters defining the dependence of the fission barrier on neutron excess are rather weak. This leads to large uncertainties in estimating the heights of the fission barriers of heavy nuclei involved in the r process. For example, it was shown in Ref. [6] that predictions on the beta-delayed fission probabilities for nuclei in the region A ~ 250 – 290 and Z ~ 92 – 98 can vary between 0% and 100% depending on the model used, thus strongly influencing the r-process termination point. Moreover, the uncertainties within the nuclear models used to calculate the fission barriers can also have important consequences on the r process. Meyer *et al.* have shown that a change of 1 MeV in the fission-barrier height can have strong influence on the production of the progenitors (A ~ 250) of the actinide cosmochronometers, and thus on the nuclear cosmochronological age of the Galaxy [12].
Recently, important progress has been made in developing full microscopic approaches to nuclear masses and fission barriers, see e.g. [13]. However, the macroscopic-microscopic approach offers some advantages for evaluating global trends, which are important for applications far from stability. We will see that this is particularly true for fission-saddle masses. In the macroscopic-microscopic approach, the smooth trends in the potential-energy landscape of the fissioning system are described by a macroscopic model based on some liquid-drop or droplet picture, while local fluctuations are calculated separately within a microscopic model using the Strutinsky method [14]. Due to the separation between macroscopic and microscopic properties of the system, this approach is very well adapted for the global description of different properties of the system not only in nuclear physics [15] but also in other fields, see e.g. [16]. The free parameters of these models are fixed using the nuclear ground-state properties and, in some cases, the height of fission barriers when available. Some examples of such calculations are shown in Figure 2 (upper part), where the fission-barrier heights given by the results of the Howard-Möller fission-barrier calculations [17, 18], the finite-range liquid drop model (FRLDM) [19], the Thomas-Fermi model (TF) [20], and the extended Thomas-Fermi model with Strutinsky integral (ETFSI) [21] are plotted as a function of the mass number for several uranium isotopes (A = 200-305). In case of the FRLDM and the TF model, the calculated ground-state shell corrections of Ref. [22] were added as done in Ref. [23]. In cases where the fission barriers were experimentally determined, the experimental values are also shown. From the figure it is clear that as soon as one enters the experimentally unexplored region there is a severe divergence between the predictions of different models.
We have performed a study on the behaviour of the fission barriers when extrapolating to very neutron-rich nuclei [10]. This study was based on the approach of Dahlinger et al. [24], where the predictions of the theoretical models were examined by means of a detailed analysis of the isotopic trends of ground-state and saddle-point masses.

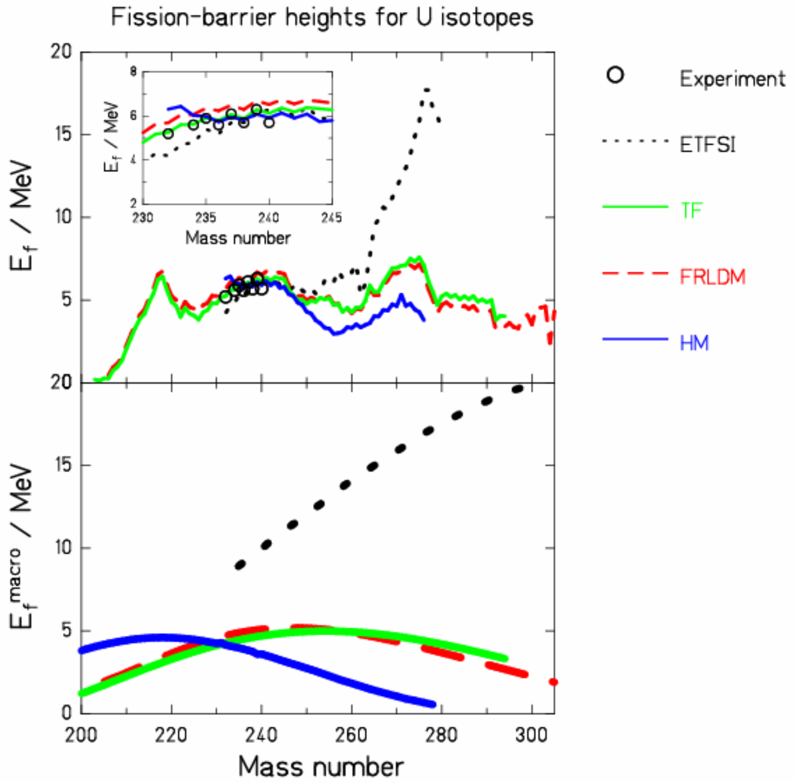

Figure 2. Full macroscopic-microscopic (upper part) and macroscopic part (lower part) of the fission barrier calculated for different uranium isotopes using: the extended Thomas-Fermi model + Strutinsky integral [21] (dotted black line), the Thomas-Fermi model [20] (full green line), the finite-range liquid-drop model [19] (dashed red line), and the Howard-Möller tables [17] (full blue line). In case of FRLDM and TF the ground-state shell corrections were taken from Ref. [22]. The small inset in the upper left part represents a zoom of the region where experimental data are available.

In order to test the consistency of these models, we study the difference between the experimental saddle-point mass $M_{sadd}^{\exp} = B_f^{\exp} + M_{GS}^{\exp}$ and the macroscopic part of the saddle-point mass $M_{sadd}^{macro} = B_f^{macro} + M_{GS}^{macro}$ given by the above-mentioned models, with B_f being the height of the fission barrier and M_{GS} the ground-state mass:

$$\delta U_{sadd} = M_{sadd}^{\exp} - M_{sadd}^{macro} = \left(B_f^{\exp} + M_{GS}^{\exp}\right) - \left(B_f^{macro} + M_{GS}^{macro}\right) \tag{1}$$

The difference between experimental and macroscopic mass, δU_{sadd} as given by Eq. 1 should correspond to the empirical shell-correction energy.

It is well known that the shell-correction energy oscillates with deformation and neutron or proton number. If we consider deformations corresponding to the saddle-point configuration, then the oscillations in the microscopic corrections for heavy-nuclei region we are interested in have a period between about 10 ~ 30 neutrons depending on the single-particle potential used, see e.g. [25, 26, 27, 28]. This means that, if we follow the isotopic trend of the shell-correction energy at the saddle point over a large enough region of neutron numbers, this quantity should show only local variations with the above given periodicity. Myers and Swiatecki gave another argument that tends to make this approach even more powerful. Theoretical considerations on the topologic properties of the fission saddle and experimental verifications suggested that the difference between the macroscopic saddle mass and the saddle mass including the influence of shell corrections is very small – below 1 – 2 MeV [20,

23, 29]. Thus, the local variations of δU_{sadd} should be very small. In other words, the saddle-point shell-correction energy as a function of neutron number should show only local, periodical, variations with small amplitude; there should be no global tendencies, e.g. increase or decrease with neutron number.
We have used this fact in Ref. [10] to test the macroscopic part of the different, above mentioned, models. Using experimental ground-state masses [30] and experimental fission barriers and different macroscopic models, we have calculated the quantity δU_{sadd} as given by Eq. 1 for a wide range of neutron numbers. If a model realistically describes the isotopic trend, the quantity δU_{sadd} will correspond to the shell-correction energy at the saddle point and will fulfil the above-mentioned condition, i.e. the slope of δU_{sadd} as a function of neutron number will be close to zero ($\partial(\delta U_{sadd})/\partial N \approx 0$). On the contrary, if a model does not describe realistically the isotopic trend, then the quantity δU_{sadd} as a function of neutron number will show global tendencies, like e.g. increase or decrease over a large range of neutron numbers ($\partial(\delta U_{sadd})/\partial N \neq 0$). Figure 3 shows the variation of δU_{sadd} for the uranium isotopic chain. Only the finite-range liquid-drop model and the Thomas-Fermi model reproduce the variation of the experimental saddle-point masses as a function of neutron number correctly, while the trends of the droplet model and the extended Thomas-Fermi model deviate from the data in opposite directions.

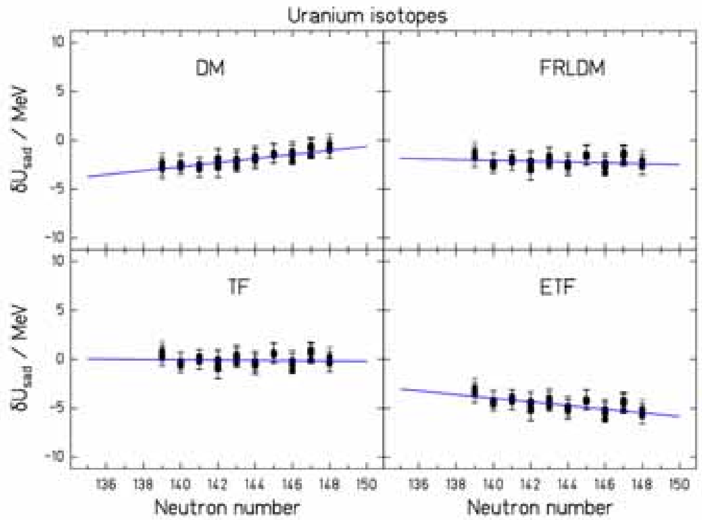

Figure 3. Difference between the experimental and the macroscopic part of the saddle-point mass calculated with the droplet model, the finite-range liquid-drop model, the Thomas-Fermi model and the extended Thomas-Fermi model for different uranium isotopes. The lines represent linear fits to the data.

The average slopes ($A_1 = \partial(\delta U_{sadd})/\partial N$) of δU_{sadd} as a function of neutron number are shown in Figure 4 versus atomic number over a range of 10 elements for the four models. For more details, see [10].
We can see from Figure 4 that the Thomas-Fermi and the Finite-range liquid drop model predict slopes which are very close to zero, while the Droplet and the extended Thomas-Fermi model result in slope values which are not consistent with zero.
The results of this study (see also [10]) show that the most realistic predictions for r-process nuclei are expected from the Thomas-Fermi model [20]. A similar conclusion can be made for the finite-range liquid-drop model [19], while further improvements in the saddle-point mass predictions of the droplet model [18] and the extended Thomas-Fermi model [21] seem to be needed.

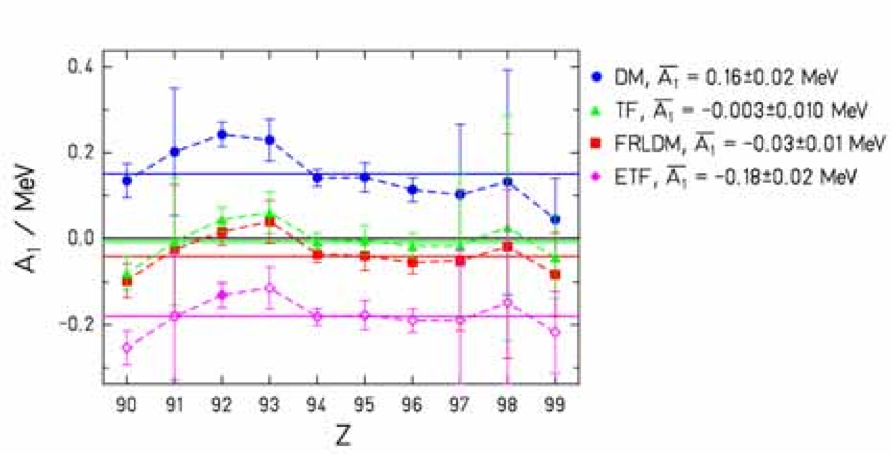

Figure 4. Average sopes of the variation of δU_{sadd} with neutron excess are shown as a function of the nuclear charge number Z obtained for the Droplet model [18] (points), the Thomas-Fermi model [20] (triangles), FRLDM [19] (squares) and the extended Thomas-Fermi model [21] (rhomboids). The full lines indicate the average values of the slopes. The average values are also given in the figure. Error bars originate from the experimental uncertainties in the fission-barrier heights. Dashed lines are drawn to guide the eye. For more details, see [10].

Mass and nuclear-charge division in fission

For understanding the role of fission in the r-process nucleosynthesis, apart from fission probabilities one also needs the masses and atomic numbers of the fragments created in the fission of heavy progenitors. For example, Qian has recently proposed that the observed structures at A~90 and A~130 in the r-process abundances in low-metallicity, old galactic halo stars can have their origin in the fission of heavy progenitors A_{prog} ~ 190 – 320 [31]. In order to test this and other similar ideas (see e.g [3, 4, 2, 7]) one needs reliable predictions on the mass and charge distributions of the fission fragments formed during the r process.

Usually it is assumed in astrophysical calculations that either both fission fragments have the same mass and the same atomic number, or that one fragment corresponds to the double-magic ^{132}Sn and the second fragment has $A = A_{prog} - 132$ and $Z = Z_{prog} - 50$. Both these assumptions are rather simplistic and not always supported by the experimental data. This can be clearly seen from Figure 5.

For the lightest nuclei shown in Figure 5, the distributions of fission fragments are symmetric. With increasing the mass of the fissionning system we observe a transition to triple- and double-humped distributions. For the heaviest systems the distributions become again symmetric, but with much smaller widths as compared to the lightest systems around astatine. If one looks at fission-fragment distributions for a given isotopic chain, for nuclei in the actinide region one can see a smooth transition from double-, to triple- and then to single-humped distributions for the lightest fissionning systems in the isotopic chain, see Figure 6. On the contrary, in case of fermium Figure 5 shows a very abrupt transition from single- to double-humped distribution when going from ^{258}Fm to ^{256}Fm.

Most of the more elaborate model descriptions of the fission process follow one of the following approaches: Either the measured observables – mass, element and kinetic energy distributions – are fitted by suitable mathematical functions with empirically determined parameters or the evolution of the fissioning system is described with a purely theoretical model. Following the first approach [32, 33], one is able to reproduce existing data very well. However, the predictive power of phenomenological models is rather low due to the lack of the essential physics.

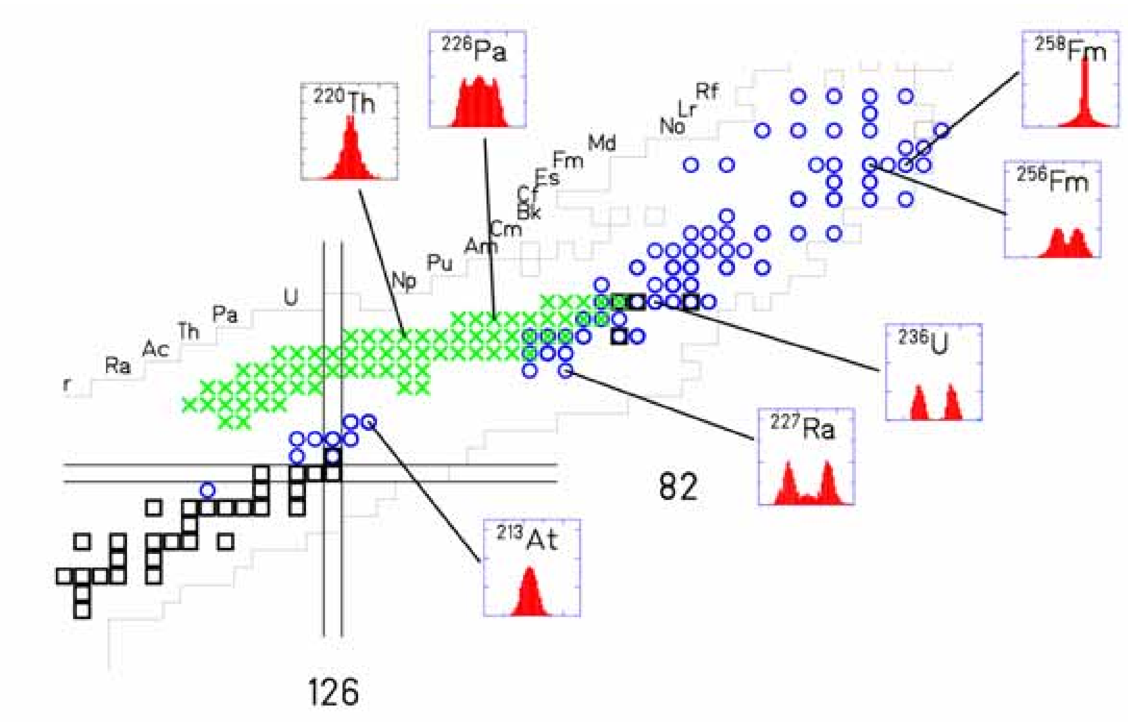

Figure 5. Available experimental data on mass or charge distributions in low-energy fission – green crosses: *Z*-distributions of fission fragments formed in fission after electro-magnetic excitations [34], blue circles: mass distributions from particle-induced and spontaneous fission. For more details, see Ref. [34]. For several compound nuclei mass or charge distributions of fission fragments are shown in small insets.

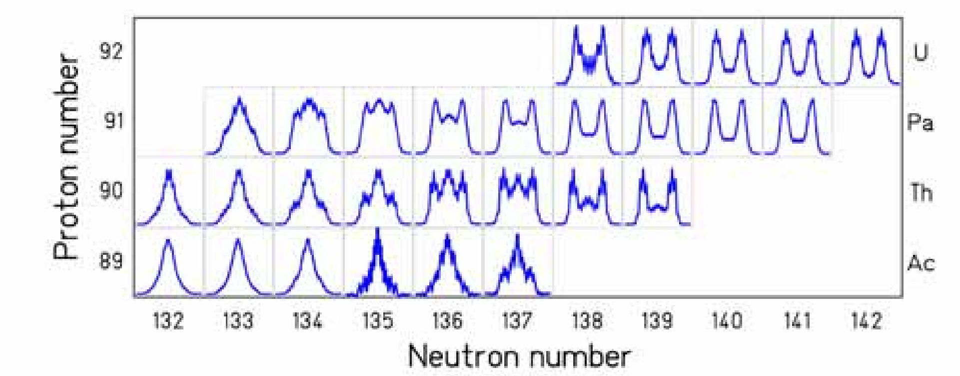

Figure 6. Element distributions observed in the fission of neutron-deficient actinides after electromagnetic excitations [34].

The second approach is very challenging: Due to the complexity of the problem, any theoretical model has to introduce a certain level of simplifications. In addition, one has to face the difficulty that the theoretical models are able to predict the relevant properties of a nuclear system only with a limited accuracy. This is obvious for the potential-energy surface in deformation space. Even in the nuclear ground-state configuration, where the single-particle structure is generally very well studied, the measured binding energies can only be reproduced with a standard deviation in the order of half an MeV. Such deviations are crucial for fission, e.g. a shift of 500 keV in the ground-state binding energy modifies the spontaneous-fission half life by about 2 orders of magnitude [35].
Recently, important progress has been made in developing a fully microscopic approach to the nuclear-fission process with inclusion of dynamic effects [36]. Using a time-dependent

formalism based on the Gaussian overlap approximation of the time-dependent generator coordinate theory and the self-consistent Hartree-Fock-Bogoliubov procedure, the authors of Ref. [36] could predict fission-fragment kinetic energies and mass distribution in the low-energy fission of ^{238}U in a rather satisfactory way. Due to the complexity of the problem, the authors have limited their approach by applying the adiabatic hypothesis, which confines their model to very low excitation energies.

Another type of theoretical models which are often used is based on the macroscopic-microscopic approach, e.g. [37, 38, 39, 40, 41, 42, 43, 44, 45]. Macroscopic-microscopic models for calculating fission-fragment properties can be divided in two groups: The first group represents fully static models, in which no dynamic effect is considered [37, 38, 39, 41, 43]. Here, the properties of fission fragments are calculated by applying the statistical model either at the saddle [43] or at the scission point [37, 38, 40]. In the second group, dynamic effects are included by using the Langevin approach for solving the equations of motion of the fissioning system [44, 45]. In this case, the challenge is to describe the influence of microscopic effects on the transport coefficients. To our knowledge, this still has not been done.

For improving our understanding of the fission process, theoretical models are mandatory. Nevertheless, due to the above-mentioned uncertainties and limitations their ability for quantitative predictions seems to be still rather restricted. Moreover, in many cases they are very time consuming which prevents their use for applications. In order to surmount these problems, we have developed a model, which combines these two approaches. Our semi-empirical model exploits several important features of the fission process according to the present theoretical understanding and at the same time makes use of the experimental information available in order to provide reliable predictions of fission-fragment nuclide distributions of nuclei far from stability. The model is imbedded in the dynamic de-excitation code ABLA [46], which considers the competition between evaporation of neutrons, light charged particles and intermediate-mass fragments on one side and fission on the other side. For excitation energies above the corresponding threshold also break-up and the simultaneous emission of several fragments is considered [47]. Fission is treated as a dynamical process, taking into account the role of dissipation in establishing quasi-equilibrium in the quasi-bound region by the implementation of a time-dependent fission-decay width [48]. When the system passes the fission barrier and proceeds to fission, it is characterised by mass and atomic number, excitation energy and angular momentum. It is the aim of our model to follow the descent from saddle to scission of the system and to predict the probability that its ends up in one of the many possible splits in Z and A. We would like to mention that preliminary versions of this model have been published previously [49, 50].

Starting with Fong [37, 38] and followed later by Wilkins et al. [40], the statistical model has been taken as the basis of most fission models that provide quantitative predictions on nuclide yields. Since the available phase space is a very important driving force of any process in nature, we consider the statistical model as the basis also of our model. Fong as well as Wilkins et al. avoided considering dynamical effects by applying the statistical model at the scission configuration. This is a rather severe simplification, which is certainly not realistic. Depending on the relaxation times of the different collective degrees of freedom, some memory on previous configurations might be present. Therefore, we will discuss this point with some care.

First we start considering fission at high excitation energy, where shells and pairing correlations are negligible. Observed mass distributions of heavy fissioning nuclei above the Businaro-Gallone point (i.e. $Z^2/A > 22$) from high excitation energies can well be described by a Gaussian distribution. This finding has been related to the available number of states above the potential energy as a function of mass asymmetry, since the potential can be approximated by a parabola near the minimum appearing at mass symmetry [51]. The second derivative $c_A = d^2U/(dA_1)^2$ of the potential as a function of the mass of one of the nascent fragments is related to the standard deviation σ_A of the mass distribution by the following relation:

$$\sigma_A{}^2 = \frac{T}{2 \cdot c_A} \tag{1}$$

T is the nuclear temperature, which is related to the excitation energy of the fissioning system $E = a\,T^2$. The coefficient a is the level-density parameter.

This relation is a very important starting point of our model. Firstly, there exists a large body of experimental data on σ_A values, which provides the empirical data basis for a realistic prediction of fission mass distributions when structural effects are negligible. Secondly, the empirical result that the variance σ_A^2 is proportional to the nuclear temperature supports the validity of the statistical model. However, it is difficult to extract from these data, at which moment on the descent from saddle to scission the decision on the width of the mass distribution is taken. We can imagine two possible extremes. In one case, the phase space at the saddle point determines the mass asymmetry of the system, which is more or less frozen on a fast descent to scission. In the other case, the mass asymmetry degree of freedom adjusts very fast to the potential and thus it is finally determined at scission. Since a variation of the mass asymmetry is connected with a substantial transport of nucleons and, thus, the inertia should be large, we tend to support the first possibility, which is also supported by Langevin calculations [52], Following this idea, we take the systematics established in Ref. [51] using the temperature at saddle in equation (1) for deducing the second derivative c_A of the potential from the experimental data. In fact, Rusanov et al. [51] deduced a direct relation of c_A with the fissility parameter Z^2/A of the fissioning nucleus. Thus, we have the first quantitative relation we use in our model to calculate the width of the mass distribution in case of sufficiently high excitation energies.

Considering the fission process at lower excitation energies, our approach has to be substantially extended in order to include the appearance of fission channels. Early ideas for this concept are formulated in Ref. [53]. Following the hypothesis that the mass asymmetry degree of freedom is essentially frozen at saddle, the probabilities for the population of the different fission channels should be decided at the outer saddle. Therefore, we assume that there is a direct correspondence between the shape of the potential at the outer saddle as a function of mass asymmetry and the population of the fission channels. The appearance of each fission channel is linked to a specific minimum in the mass-asymmetry dependent potential at the outer saddle. At this stage we empirically determine the depths and the widths of potential minima of the different fission channels by the weights and the widths of the corresponding components in the empirical nuclide distributions. For this purpose, we need to calculate the number of states available in the different potential minima. This time, the Fermi-gas level density is not realistic: We have to consider the level density in a configuration with a substantial shell effect. For this purpose, we use the analytical relation proposed by Ignatyuk et al. [54].

The description of Ignatyuk et al. requires the knowledge of the macroscopic potential. According to the previous discussion, we represent it by the parabolic potential deduced by Rusanov et al. [51] from the widths of the mass distributions at high excitation energies.

We consider the mass distribution of the fission fragments from ^{238}U(n,f) as the key information for the quantitative determination of the shell effects at the outer barrier. As demonstrated in Figure 7, one obtains a rather consistent description, which reproduces the decrease of the relative population of the asymmetric fission channels with increasing excitation energy just by introducing two shells corresponding to the Standard 1 and Standard 2 fission channels [55], and by considering the washing out of the shell effects with increasing excitation energy.

Up to now, the shells at the outer barrier are formulated as a function of mass asymmetry. At this stage, we have a look to the results of shell-model calculations with the two-centre shell model [56], respectively Cassini shapes [57]. They reveal that the shell effects at the outer barrier in ^{238}U are qualitatively similar to the shells in the separate fragments. It seems that the structure of the wave functions is quite similar all the way from the outer saddle to scission [58]. This is not valid any more for more compact shapes, since the energetically favoured shape at the inner saddle is triaxial and mass-symmetric. Thus, we can profit from the investigations of Wilkins et al. [40] on the scission-point configuration, who stated that the most important shells behind the Standard 1 fission channel are N = 82 and Z = 50, while the Standard 2 fission channel is related to the $N \approx 90$ strongly deformed shell. Following these ideas, we attribute the two mass-asymmetric fission channels to the shells in the nascent heavy fragment mentioned above, while we neglect the influence of shell effects in the light fragment. From our adjusted parameters it appears that the spherical N = 82 and Z = 50 shells are considerably weaker than the shell effects we know from the ground-state masses around ^{132}Sn. It might be assumed that the additional matter in the neck disturbs the symmetry of the nascent heavy fragment and reduces the shell gaps compared to the ideal spherical configuration we meet in ^{132}Sn. The dominating appearance of the Standard 2 fission channel in ^{238}U(n,f) seems to indicate that the deformed $N \approx 90$ shell, which appears less strong in the separate fragments, see the results of the shell-model calculations in Ref. [40], is less affected by the neck. Also the deviation of the N/Z ratio of ^{132}Sn from the corresponding value of the fissioning nucleus weakens the influence of the Standard I fission channel.

For completeness, we would like to mention that the model not only describes mass distributions but also considers the charge polarization in the nuclide production. Since there is only very little nucleon exchange necessary to exploit the full variation in N/Z to be expected, we assume that the charge polarization is determined near scission. Quantitatively, the charge polarization is governed by the macroscopic contributions to the energy at scission [59] in most cases. Only the simultaneous influence of the Z = 50 and N = 82 shells leads to a rather important deviation from this trend for the Standard 1 fission channel, which tends to produce nuclides closer to the doubly magic ^{132}Sn. The width of the charge distribution for constant mass split is determined in analogy to equation (1), inserting the temperature and the curvature of the potential for charge polarization at scission.

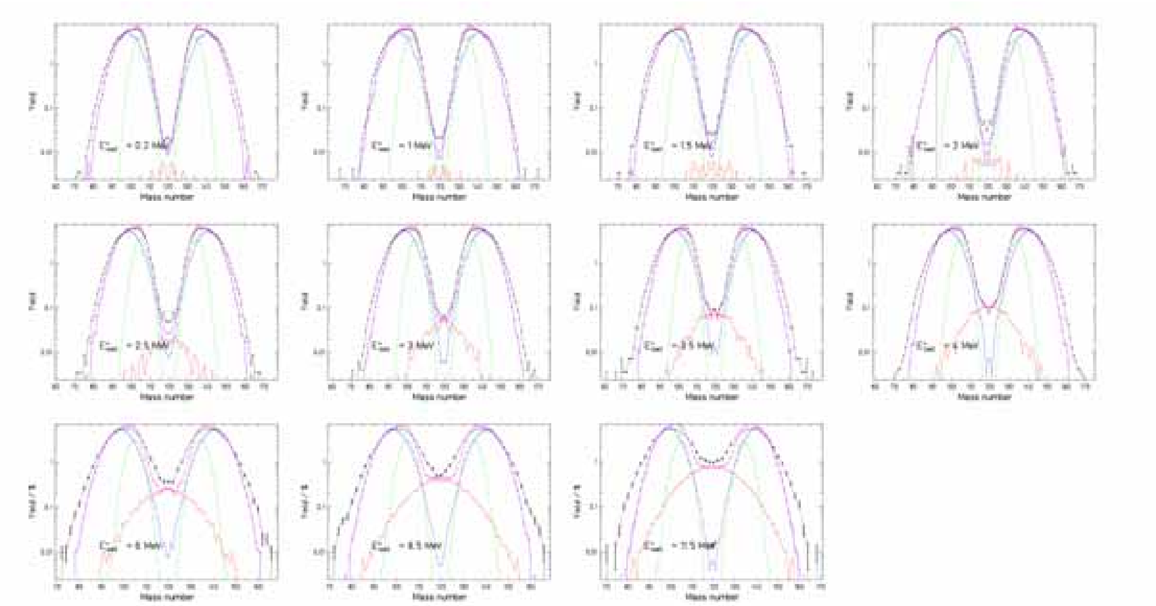

Figure 7. Calculated mass distributions (pink symbols) for neutron-induced fission of ^{238}U in comparison with experimental data (black symbols) [60, 61] for different values of the excitation energy above the fission saddle of the composite system ^{239}U. The calculated individual contributions of the different fission channels are shown in addition: Standard 1 (green), Standard 2 (blue), and Superlong (orange).

After having adjusted the strengths and the widths of the three shells to the mass distributions of the system ^{238}U(n,f), we are interested to check the predictive power of the model by applying it to other systems.

As an example for the application of this approach, we show in Figure 8 the model-calculated element distributions of fragments formed in the electromagnetic-induced fission of several secondary beams ranging from ^{220}Ac to ^{234}U. They compare rather well with the experimental data, shown in Figure 6. The transition from single- to triple- and then to double-humped fragment distributions is correctly described by the model. Please note, that all calculations were performed with one and the same set of model parameters; no adjustment to individual systems has been done. In particular, the parameters of the shells of the nascent fragments are exactly the same for all systems. Considering this success, we conclude that our model has a remarkable predictive power, once the parameters have carefully been deduced from experimental fission-fragment distributions. This gives us confidence when extrapolating into regions where no experimental data are available. In case of r-process simulations, the model was applied in Ref. [9].

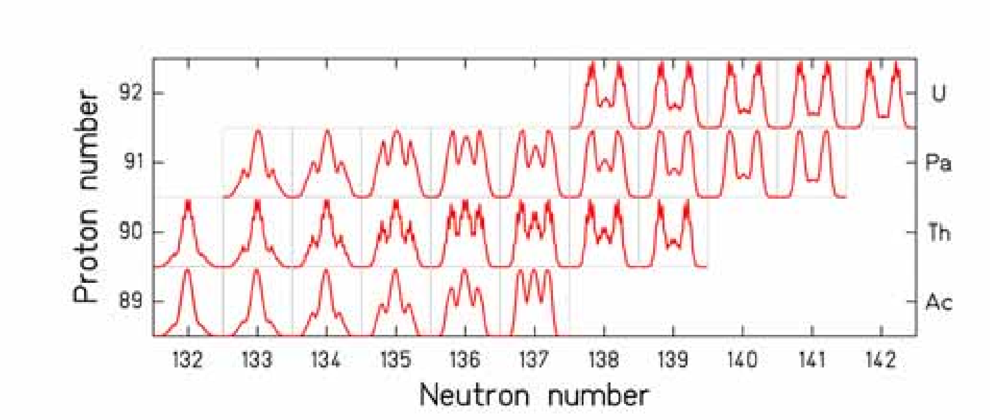

Figure 8. Calculated fission-fragment nuclear-charge distributions in the range *Z* = 24 to *Z* = 65 from ^{220}Ac to ^{234}U in electromagnetic-induced fission shown on a chart of the nuclides.

We would like to stress that the most salient feature of our model represent a rather peculiar application of the macroscopic-microscopic approach to nuclear properties. In our consideration of the properties of the fissioning system at the saddle configuration, we attribute the macroscopic properties to the strongly deformed fissioning system, while the microscopic properties are attributed to the shell structure in the nascent fragments. This way, the macroscopic and the microscopic properties are strongly separated, and the number of free parameters is independent from the number of systems considered.

Conclusions

In this contribution, we have discussed the status of present experimental and theoretical knowledge on some aspects of fission which are important input for the r-process calculations. We have specifically concentrated on the height of the fission barrier and on fragment formation in fission.
Using available experimental data on fission barriers and ground-state masses, we have presented a detailed study of the predictions of different models concerning the isospin dependence of saddle-point masses. Evidence is found that several macroscopic models yield unrealistic saddle-point masses for very neutron-rich nuclei, which are relevant for the r-process nucleosynthesis.
We have also discussed different approaches used to calculate fission-fragment distributions. Empirical systematics are not suited for astrophysical applications. Theoretical approaches still fail to include all important features of the fission process, but they can give good orientation of major trends. A macroscopic-microscopic approach based on macroscopic properties of the fissioning system and microscopic properties of the nascent fission fragments with schematic considerations of dynamical features seems to be a promising tool for robust extrapolations of empirical features.
On the experimental level there is little hope to obtain direct information on the fission properties of the heavy nuclei on the r-process path in the near future. However, novel experimental installations, like the electron-ion collider (ELISE) project [62] at GSI, may contribute essentially to widen the empirical knowledge to more exotic nuclei and thus are expected to improve our empirical basis for predictions and extrapolations needed as an input of r-process network calculations.
Acknowledgments. We are in debt to Karlheinz Langanke, Gabriel Martinez-Pinedo and Nikolaj Zinner for fruitful discussions concerning the r process.

References

[1] J. J. Cowan, F.-K. Thielemann, J. W. Truran, Phys. Rep. **208** (1991) 267.
[2] I. Panov et al., Nucl. Phys. **A 747** (2005) 633
[3] P. A. Seeger, W. A. Fowler, D. D. Clayton, Astrop. J. **11** Suppl. (1965) S121
[4] T. Rauscher, J. H. Applegate, J. J. Cowan, F.-K. Thielemann, M. Wiescher, Astrop. J. **429** (1994) 49
[5] F. K. Thielemann, J. Metzinger, H. V. Klapdor-Kleingrothaus, Z. Phys. **A 309** (1983) 301
[6] I. V. Panov, F.-K. Thielemann, Astron. Lett. **29** (2003) 510

[7] I. V. Panov, E. Kolbe, B. Pfeiffer, T. Rauscher, K.-L. Kratz, F.-K. Thielemann, Nucl. Phys. **A 747** (2005) 633
[8] E. Kolbe, K. Langanke, G. M. Fuller, Phys. Rev. Lett **92** (2004) 111101
[9] A. Kelić, N. Zinner, E. Kolbe, K. Langanke, K.-H. Schmidt, Phys. Lett. **B 616** (2005) 48
[10] A. Kelić, K.-H. Schmidt, Phys. Lett. **B 643** (2006) 362
[11] http://www-nds.iaea.org/RIPL-2/
[12] B. S. Meyer, W. M. Howard, G. J. Mathews, K. Takahashi, P. Möller, G. A. Leander, Phys. Rev. **C 39** (1989) 1876
[13] J. M. Pearson, S. Goriely, Nucl. Phys. **A 777** (2006) 623
[14] V. M. Strutinsky, Nucl. Phys. **A 95** (1967) 420
[15] J. R. Nix, P. Möller, Proc. Int. Conf. on Exotic Nuclei and Atomic Masses (ENAM 95), Arles, France, 1995 (Les Editions Frontières, Gif sur Yvette, 1995)
[16] B. Agoram, V. H. Barocas, Journ. Biomech. Eng. **123** (2001) 362
[17] W. M. Howard, P. Möller, At. Data Nucl. Data Tables **25** (1980) 219
[18] W. D. Myers, „Droplet Model of Atomic Nuclei“, 1977 IFI/Plenum, ISBN 0-306-65170-X
[19] A. J. Sierk, Phys. Rev. **C 33** (1986) 2039
[20] W. D. Myers, W. J. Swiatecki, Phys. Rev. **C 60** (1999) 014606-1
[21] A. Mamdouh, J. M. Pearson, M. Rayet, F. Tondeur, Nucl. Phys. **A 679** (2001) 337
[22] P. Möller, J. R. Nix, W. D. Myers, W. J. Swiatecki, At. Data Nucl. Data Tables **59** (1995) 185
[23] W. D. Myers, W. J. Swiatecki, Nucl. Phys. **A 601** (1996) 141
[24] M. Dahlinger, D. Vermeulen, K.-H. Schmidt, Nucl. Phys. **A 376** (1982) 94
[25] D. Scharnweber, U. Mosel, W. Greiner, Phys. Rev. Lett. **24** (1970) 601
[26] M. Bolsterli, E. O. Fiset, J. R. Nix, J. L. Norton, Phys. Rev. **C 5** (1972) 1050
[27] P. Möller, J. R. Nix, „Physics and Chemistry of Fission“, Proceedings of a conference at Rochester (IAEA, Vienna 1974), Volume 1, page103.
[28] J. Randrup, S. E. Larson, P. Möller, S. G Nilsson, K. Pomorski, A. Sobiczewski, Phys. Rev. **C 13** (1976) 229
[29] K. Siwek-Wilczyńska, I. Skwira, J. Wilczyński , Phys. Rev. **C 72** (2005) 034605
[30] G. Audi, A. H. Wapstra, C. Thibault, Nucl. Phys. **A 729** (2003) 337
[31] Y.-Z. Qian, Astr. J. **569** (2002) L103
[32] F. Atchison, Jül-Conf-34 KFA-Jülich, Germany (1980), p. 17
[33] V. A. Rubchenya, J. Äystö, Nucl. Phys. **A 701** (2002) 127
[34] K.-H. Schmidt et al., Nucl. Phys. **A 665** (2000) 221
[35] Z. Patyk et al., Nucl. Phys. **A 491** (1988) 267
[36] H. Goutte, J. F. Berger, P. Casoli, D. Gogny, Phys. Rev. **C 71** (2005) 024316
[37] P. Fong, Phys. Rev. **102** (1956) 424
[38] P. Fong, Phys. Rev. **C 17** (1978) 1731.
[39] A. S. Jensen, T. Dossing, Proc. IAEA Symp. on Physics and Chemistry of Fission, 1973, Rochester, (1974), IAEA Vienna, vol. I, p. 409-420
[40] B. D. Wilkins, E. P. Steinberg, R. R. Chasman, Phys. Rev. **C 14** (1976) 1832
[41] U. Brosa, S. Grossmann, A. Müller, Phys. Rep. **197** (1990) 167
[42] P. Möller, D. G. Madland, A. J. Sierk, A. Iwamoto, Nature **409** (2001) 785
[43] M. C. Duijvestijn, A. J. Koning, F.-J. Hambsch, Phys. Rev. **C 64** (2001) 014607
[44] T. Asano et al, J. Nucl. Radiochem. Sciences **5** (2004) 1
[45] Y. Aritomo, M. Ohta, Phys. Atom. Nucl. **66** (2003) 1105
[46] M. V. Ricciardi et al., Phys. Rev. **C 73** (2006) 014607.
[47] K.-H. Schmidt et al., Nucl. Phys. **A 710** (2002) 157.
[48] B. Jurado et al., Nucl. Phys. **A 747** (2005) 14
[49] J. Benlliure, A. Grewe, M. de Jong, K.-H. Schmidt, S. Zhdanov, Nucl. Phys. **A 628** (1998) 458
[50] K. Kruglov et al., Eur. Phys. J. **A 14** (2002) 365.
[51] Ya. Rusanov et al., Phys. At. Nucl. **60** (1997) 683
[52] P. N. Nadtochy, G. D. Adeev, A. V. Karpov, Phys. Rev. C 65 (2002) 064615
[53] M. G. Itkis et al., Sov. J. Nucl. Phys. **43** (1986) 719.
[54] A. V. Ignatyuk, G. N. Smirenkin, A. S. Tiskin, Yad. Fiz. **21** (1975) 485 (Sov. J. Nucl. Phys. **21** (1975) 255)
[55] K.-H. Schmidt et al., arXiv:nucl-ex/0711.3967
[56] J. Maruhn, W. Greiner, Z. Phys. **251** (1972) 431

[57] V. V. Pashkevich, Nucl. Phys. **A 477** (1988) 1
[58] U. Mosel, H. W. Schmitt, Nucl. Phys. **A 165** (1971) 73.
[59] P. Armbruster, Nucl. Phys. **A 140** (1970) 385.
[60] F. Vivès et al. Nucl. Phys. **A 662** (2000) 63.
[61] C. M. Zöller, PhD thesis, Technical University Darmstadt, 1995
[62] ELISE, http://www.gsi.de/fair/experiments/elise/